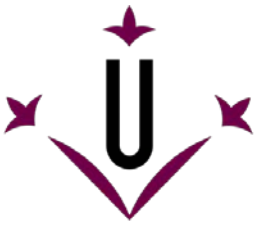

# SHOULD ENERGY OUTPUT BE PREFERRED OVER CONVERSION EFFICIENCY TO QUALIFY ADVANCED MULTI-JUNCTION SOLAR CELLS?

Alexis Vossier[1], Alberto Riverola[2], Daniel Chemisana[2], Alain Dollet[1] and Christian A. Gueymard[3]

[1]CNRS-PROMES, 7 Rue du Four Solaire, 66120 Odeillo, France

[2]University of Lleida, c/ Pere de Cabrera s/n, 25001, Lleida, Spain

[3]Solar Consulting Services, Colebrook, NH, USA

## Abstract

For better conversion of sunlight into electricity, advanced architectures of multi-junction (MJ) solar cells include increasing numbers of subcells. The Achilles' heel of these cells lies in their increased sensitivity to the spectral distribution of sunlight, which is likely to significantly alter their performance during real working operation. This study investigates the capacity of MJ solar cells comprising up to 10 subcells to accommodate a wide range of spectral characteristics of the incident radiation. A systematic study is performed, aimed at a realistic estimation of the energy output of MJ-based concentrating photovoltaic (CPV) systems at characteristic locations selected to represent a large range of climatic conditions. We show that optimal MJ architectures could have between 4 and 7 subcells. Beyond 7 subcells, the slight gains in peak efficiency are likely outweighed by detrimental increases in dependence on local conditions and in annual yield variability. The relevance of considering either conversion efficiency or modeled energy output as the most appropriate indicator of the cell performance, when considering advanced architectures of MJ solar cells, is also discussed.

## 1. Introduction

Multi-junction (MJ) solar cells are currently seen as one of the most promising options towards reaching ultra-high solar-to-electricity conversion efficiencies [1]. Today's state-of-the-art MJ solar cells include up to 5 different subcells, reaching efficiencies approaching 50% (The world record is currently held by a quadruple-junction solar cell with a conversion efficiency of 46% under concentrated sunlight [2]).

Increasing the efficiency of MJ cells is basically achieved by increasing the number of *pn* junctions involved in the stack, allowing a more efficient absorption of the solar spectrum and thus, higher conversion efficiencies. However, growing multiple subcells on top of each other is a quite challenging task, due to the constraints imposed by lattice matching, current matching, as well as the materials properties, which need to be suitable both in terms of optical properties (electronic gap) and electrical properties (diffusion length). Nonetheless, significant progress has been achieved, and cell manufacturers are now able to grow MJ solar cell architectures containing up to 5 different subcells [3].

It is stressed, however, that ever increasing the number of subcells in a MJ stack is not necessarily ideal, for two major reasons:

1) First, the extra cost associated with the growth of a supplementary *pn* junction is not necessarily counter-balanced by a sufficient gain in efficiency of the device. In reality, the gain in efficiency brought by the addition of a supplementary subcell decreases when the number of subcells in the stack increases. Adding a supplementary subcell does provide a real boost in efficiency when considering cell structure involving only very few subcells. For instance, the maximum theoretical efficiency of a tandem cell is 33.5% higher than the maximum theoretical efficiency of a single junction solar cell, but adding a 10th subcell to a conceptual 9-junction solar cell would only lead to less than 1% increase in efficiency [4][5][6].

2) Second, the sensitivity of MJ solar cells to variations in the irradiance's spectral distribution has been shown to be more pronounced for cell architectures involving a large number of subcells [6]. In particular, variations in the spectral distribution of sunlight—due to absorption and reflection processes in optical elements, or variations in air mass (AM)—may significantly alter the performance of the system relative to the performance expected when using the spectrum for which the cell was tailored, especially for MJ stacks containing 4 subcells or more.

This last point raises the question of whether or not Concentrating Photovoltaic (CPV) systems involving advanced architectures of MJ solar cells are likely to outperform simpler PV devices, taking into account the typical variations in working conditions over a long period of time. In order to answer this question, a systematic performance study is conducted here, aimed at estimating the annual energy yield of CPV systems based on MJ solar cells involving up to 10 subcells.

## 2. Calculation method

The numerical method used here is based on the detailed balance model originally suggested by Shockley and Queisser (SQ) in 1961 [7], which has been described in detail elsewhere [8].

Basically, the maximum electrical power that can be extracted from a solar cell is obtained as the difference between the absorbed and emitted radiation. Both are conveniently described by the generalized Planck's law, as pointed out in [8].

The maximum current ($I$) extractable from the cell can be obtained from:

$$I/q = \dot{N}_S - \dot{N}_R \quad (1)$$

where $q$ is the elementary charge, and $\dot{N}_S$ and $\dot{N}_R$ are the current contributions associated

with the absorption and emission of photons, which both are a function of the semiconductor bandgap, cell and sun temperatures, and other parameters, as described in [6]. Using the SQ limit, the ultimate efficiency is given by the next equation, where $P_{in}$ is the incident power:

$$\eta_{SQ} = \frac{\left\{qV\left[\dot{N}_S(\mu = 0) - \dot{N}_R(\mu = qV)\right]\right\}_{\max}}{P_{in}} \qquad (2)$$

The "ideal" solar cell, as described by SQ, is based on several assumptions:

- Each absorbed photon generates one single electron-hole pair.
- There is no absorption of photons with energy less than the semiconductor band gap.
- The only recombination process within the cell is radiative recombination; the other non-radiative processes (SRH, Auger) are thus neglected.
- The resistive losses are assumed to be zero.
- The cell temperature is kept equal to the ambient temperature (298 K).

Using this model, it is possible to derive the combination of electronic gaps leading to an optimum solar-to-electricity conversion for a given set of working conditions ($T_c$, $f(\lambda)$, and $X$), where $T_c$ denotes the cell temperature, $f(\lambda)$ the spectral distribution of sunlight, and $X$ the concentration ratio of the irradiance to which the cell is submitted. Table 1 summarizes the optimum efficiencies and bandgaps for MJ solar cells comprising up to 10 subcells, assuming a cell temperature of 298 K, an AM1.5D solar spectrum, and an illumination power equivalent to 1 sun.

Table 1: Optimum efficiencies and bandgap energies, $E_g$, (eV) for MJ solar cells comprising up to 10 subcells, under the AM1.5D spectrum and for 1-sun illumination [1].

| Spectrum | Nb. Cells | $E_{g1}$ | $E_{g2}$ | $E_{g3}$ | $E_{g4}$ | $E_{g5}$ | $E_{g6}$ | $E_{g7}$ | $E_{g8}$ | $E_{g9}$ | $E_{g10}$ | Efficiency (%) |
|---|---|---|---|---|---|---|---|---|---|---|---|---|
| AM1.5D | 1 | 1.14 | | | | | | | | | | 33.2 |
| | 2 | 1.57 | 0.94 | | | | | | | | | 45.1 |
| | 3 | 1.75 | 1.18 | 0.7 | | | | | | | | 50.7 |
| | 4 | 1.94 | 1.44 | 1.05 | 0.7 | | | | | | | 54.4 |
| | 5 | 2.07 | 1.61 | 1.26 | 0.99 | 0.7 | | | | | | 56.6 |
| | 6 | 2.18 | 1.74 | 1.44 | 1.17 | 0.95 | 0.68 | | | | | 58.7 |
| | 7 | 2.27 | 1.85 | 1.56 | 1.33 | 1.12 | 0.92 | 0.7 | | | | 59.8 |
| | 8 | 2.29 | 1.88 | 1.59 | 1.37 | 1.16 | 0.96 | 0.74 | 0.5 | | | 60.8 |
| | 9 | 2.35 | 1.96 | 1.69 | 1.47 | 1.26 | 1.09 | 0.94 | 0.74 | 0.53 | | 61.4 |
| | 10 | 2.41 | 2.03 | 1.77 | 1.56 | 1.39 | 1.21 | 1.05 | 0.92 | 0.74 | 0.55 | 62 |

The spectral distribution of the incident irradiance to which solar cells are submitted under real working operations may differ significantly from the AM1.5D reference spectrum. Consequently, MJ solar cells should be qualified not only for their ability to achieve high solar-to-electricity conversion efficiencies under standard conditions, but also for their capacity to generate electrical power when exposed to sunlight whose spectral distribution differs from them. In order to tackle the latter issue, the energy output of a CPV system involving MJ cell architectures optimized for AM1.5D spectrum (Table 1) is estimated over a full year in what follows, using as input the (variable) spectral distribution of sunlight at various representative locations around the globe, and assuming a concentration ratio of 1000 sun (where 1 sun = 1000W/m²). For simplification purposes, it is assumed that the concentrator optics does not alter the incident spectrum. Of course, this is not always practically the case [6], but the present work only aims at showing the typical trends induced by spatio-temporal variations in atmospheric parameters. The energy generated by the CPV system is finally estimated using a trapezoidal integration method, described elsewhere [9].

## 3. Atmospheric variables

The atmospheric variables that mostly affect the solar spectrum characteristics—and thus the CPV cell performance—are the air mass (AM), aerosol optical depth (AOD or $\tau$) and precipitable water (PW). Air mass is defined as the distance, relative to the shortest (vertical) path length, that the sunrays traverse through the atmosphere before impacting the Earth's surface. AM is the variable to which the spectrum is normally the most sensitive.

AOD characterizes the radiative strength of aerosols (urban haze, smoke particles, desert dust, sea salt…) in the vertical direction. The Ångström law links the AOD at wavelength ($\lambda$) to that at $\lambda$ = 1μm (also known as the Ångström turbidity coefficient $\beta$) and to the Ångström exponent ($\alpha$) through the equation:

$$\tau = \beta\lambda^{-\alpha} \qquad (3)$$

Values of $\alpha$ greater than 2 indicate the presence of fine particles (e.g., smoke particles or sulphates), whereas values close to zero are typically related to the presence of coarse particles, such as sea salt or desert dust [10]. $\alpha$ can be viewed as a single parameter suitable for a large bandwidth between e.g. 440 and 870 nm, or alternatively can be subdivided into two sub-indicators: $\alpha_1$ for wavelengths < 500 nm and $\alpha_2$ for wavelengths ≥ 500 nm [11].

Finally, PW is the amount of condensed water (expressed here in cm) corresponding to the total water vapor contained in a vertical atmospheric column above any location. Water vapor has strong absorption bands in the near infrared, which directly impacts the spectrum.

## 4. Impact of atmospheric variables on the solar spectrum

In order to display the individual spectral effect of the atmospheric parameters in a representative and intuitive manner, the Spectral Irradiance Impact (SII) indicator is proposed as follows:

$$SII(\lambda) = \frac{\int_{\lambda}^{\lambda+d\lambda} \left( E_{AM1.5\,ASTMG173(\lambda)}\Big|_{(AM|PW|AOD)} - E_{AM1.5\,ASTMG173(\lambda)} \right) d\lambda}{\int_{\lambda_{min}}^{\lambda_{max}} E_{AM1.5\,ASTMG173(\lambda)}\, d\lambda} * 100 \quad (4)$$

In essence, SII expresses the relative difference between the modified spectrum obtained by altering the reference spectrum (AM1.5D from ASTM G173) through the variation of one of the three main atmospheric variables (AM, PW or AOD) at a time, and the AM1.5D reference spectrum. This difference is normalized to the total irradiance of the reference spectrum in the range of wavelengths at which the PV cell operates, namely $\lambda_{min}$ = 300 nm and $\lambda_{max}$ = 2500 nm. This specific indicator estimates the amplitude of the spectral "disturbance" with respect to the total irradiance, allowing an estimation of the extent to which each atmospheric parameter affects each waveband of the solar spectrum. Such an indicator is helpful to better grasp how the different subcells in MJ stacks might be affected by variations in the different spectral characteristics studied here. The analysis is conducted using the Simple Model of the Atmospheric Radiative Transfer of Sunshine (SMARTS 2.9.5) [12]. First, the parameters defined as reference values by the standard AM1.5D spectrum from ASTM G173 are assigned [13]. Then, one of the atmospheric variables is varied within a realistic range, keeping the others fixed at their reference value. The SII indicator is thus calculated, and a contour graph for each parameter is plotted along with the reference spectrum, thus providing an illustrative representation of the affected bandwidths (Figures 1–3). The black horizontal line corresponds to the reference value of the atmospheric variable of interest used to obtain the reference spectrum (AM=1.5, $AOD_{500}$ = 0.084 and PW = 1.416 cm) [13]. The impact of each major atmospheric variable is described in the next subsections.

### 4.1 *Air mass*

Figure1 depicts the effects on the solar spectrum of varying AM, which occurs during any day since AM is just a direct function of the sun's zenith angle (*Z*). The relative air mass is varied here from 1 (Z=0º) to 7 (Z=82.2º) in agreement with equation (5) [12].

$$AM = [cosZ + 0.45665Z^{0.07}(96.4836 - Z)^{-1.6970}]^{-1} \quad (5)$$

Light scattering caused by all atmospheric molecules (such as nitrogen and oxygen, which make up most of the atmosphere) is particularly strong in the blue part of the spectrum

(due to the fact that Rayleigh scattering is more effective at shorter wavelengths, considering its $\lambda^{-4}$ dependence). As a consequence, the penalty associated with increasing AM is significant in this spectral region. The decrease in the spectral irradiance is found particularly strong in the spectral region where the sun emits the highest power density, with a peak attenuation occurring around 450 nm.

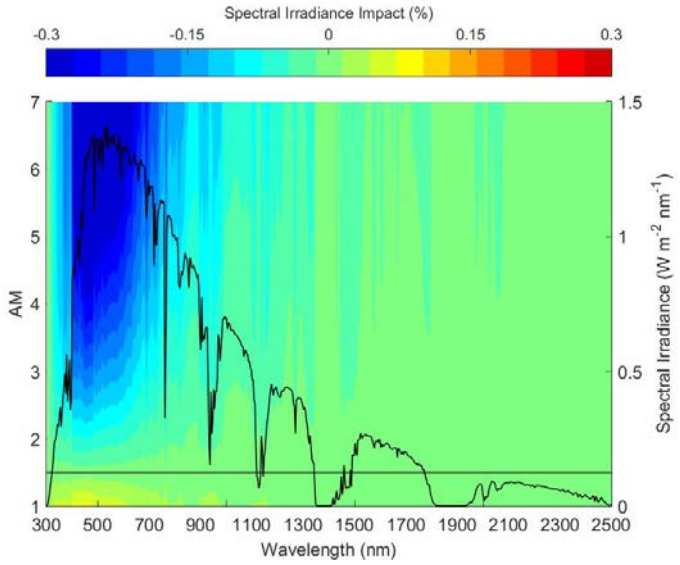


Figure. 1. Spectral Irradiance Impact as a function of air mass.

### 4.2 *Aerosol optical depth*

As previously stated, AOD is related to the amount of solar radiation attenuated because of fine particles. Considering the typical wavelength dependence described by Eq. (3), the aerosol attenuation mainly occurs at short wavelengths.

Figure 2 shows the influence of AOD on spectral irradiance, relative to the standard AM1.5D ASTM G173 reference spectrum. The AOD at 500 nm, $AOD_{500}$, is varied here from 0 (ideally clean atmosphere) to 1 (highly turbid conditions). Extreme and rare conditions, when $AOD_{500}$ can reach 3.0 or more, are not considered for clarity. The amplitude with which AOD affects the solar spectrum is similar to the AM effect reported in Fig. 1. However, the wavelength extent over which AOD causes noticeable degradation in the spectral irradiance is more restricted. In particular, no measurable effect can be noticed in the mid-IR region (above 1800 nm), as opposed to AM.

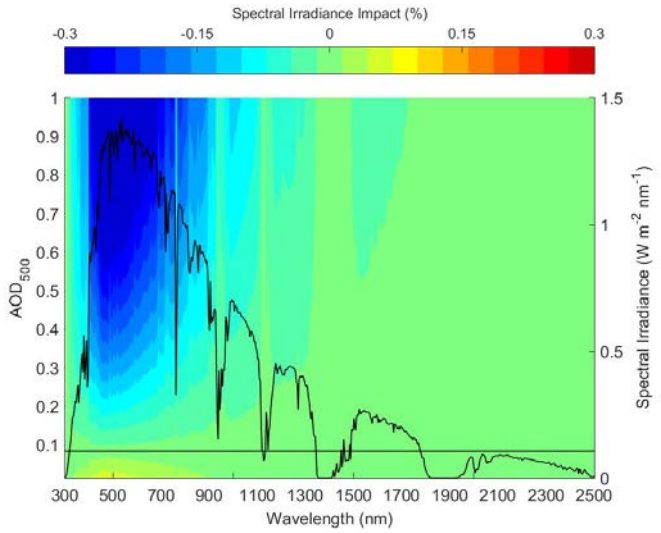


Figure. 2. Spectral Irradiance impact as a function of AOD.

Similar calculations have been performed in order to grasp the extent to which variations from 0 to 2.5 in the Ångström exponent may affect the spectral irradiance impact. Even though $\alpha$ is known to have a significant impact on direct normal irradiance (DNI) and on parts of the spectrum, its impact on SII is typically only one order of magnitude lower than that of AOD depicted in Fig. 2, with spectral irradiance impact values lower than ±0.025%, even for the most extreme values of $\alpha$.

### 4.3 *Precipitable water*

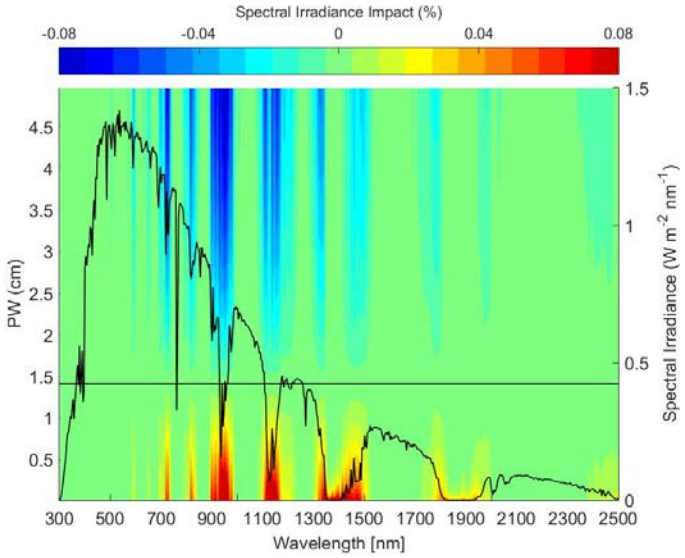


Figure. 3. Spectral Irradiance impact as a function of PW.

Contrarily to AM and AOD, which both affect most of the shortwave spectrum, PW impacts it only in specific absorption bands. Outside of these bands, its effect may be

considered negligible. PW may vary from ≈0 (ideally dry atmosphere) to ≈9 (highly wet tropical atmosphere). For simplicity, the extreme conditions above 5 cm are not considered further. The water vapor absorption bands are mainly located in the near-infrared and infrared regions of the spectrum. As can be observed in Fig. 3, the higher impact on SII occurs around 940, 1100 and 1400 nm. Overall, the impact of PW on SII is smaller than that of AM or AOD by more than a factor of 2.

## 5. Impact of atmospheric parameters on the efficiency of MJ cells

Figures 1–3 exemplify the impact of the three main atmospheric variables on the incident spectrum. In turn, these changes in spectral distribution can be expected to have potential effects on the power output of MJ cells, depending on their spectral response. These effects are characterized in more detail in what follows, based on the model described in Section 2.

### 5.1 *Impact of Air Mass*

PV cells are usually designed and rated assuming a spectral distribution of sunlight described by the appropriate AM1.5 reference spectrum. However, under real working conditions, solar cells might be subjected to variance in the distribution of the incident spectrum, because (i) the location of the installed system experiences different atmospheric conditions than those assumed in the standard, on average; and (ii) seasonal variations both in the sun's position (and thus AM) and in atmospheric conditions. All these factors give rise to substantial temporal variations in the actual spectrum to which the cell is exposed on an instantaneous basis. The overall annual effect can only be predicted through detailed simulation.

It is known that the power response of a CPV module comprising conventional triple-junction solar cells is drastically reduced when exposed to AM values exceeding 1.5 [9]. The ability of MJ solar cells to accommodate changes in DNI's spectral distribution has also been questioned [6]. Remarkably, such changes were demonstrated to have a strong negative impact on the conversion efficiency of solar cells involving 3 subcells or more.

Figure 4 shows the conversion efficiency of MJ solar cells based on the AM1.5D-optimized standard design, and comprising up to 10 subcells, when exposed to AM values between 1 and 7.

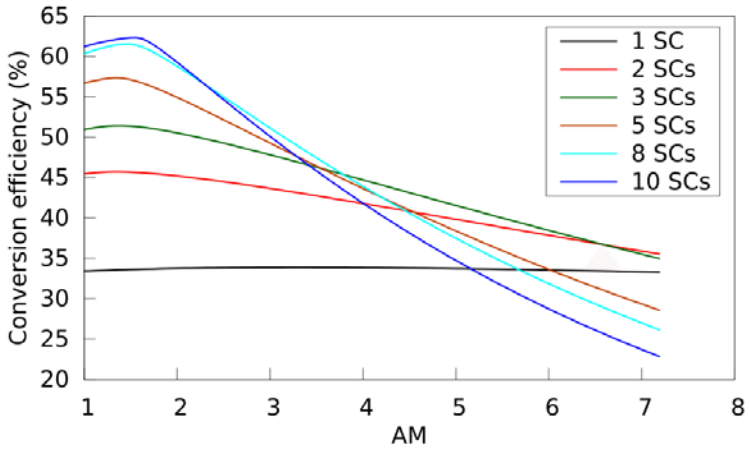


Figure. 4. Conversion efficiency of "AM1.5D-optimized" MJ Solar cells comprising up to 10 subcells (SC) as a function of Air Mass (AM).

Single-junction solar cells show constant conversion efficiency as a function of AM, assuming all other atmospheric conditions are maintained at their reference value. This stability stresses the intrinsic ability of these structures to withstand changes in the incident spectrum without degradation in their conversion efficiency. Conversely, MJ solar cells demonstrate a strong sensitivity to AM. Most importantly, the efficiency degradation's magnitude increases with the number of subcells in the stack. MJ solar cells involving 2 or 3 subcells show a limited degradation for AM in the 1–3 range, typical of real operating conditions. The decrease in conversion efficiency is then no more than 3% below the maximum efficiency. Beyond AM=3, however, sharp degradation in conversion efficiency occurs. This is representative of high latitudes, winter season, or daily instants close to sunrise and sunset times. This trend is exacerbated by the number of subcells. For 5 subcells or more, a pronounced drop in conversion efficiency is obvious, even for AM values close to the "design AM" value of 1.5. These results suggest that, although the peak efficiency can be increased by adding subcells, it then becomes a transient—rather than stable and unequivocal—characteristic of the MJ cell.

This behavior is consistent with the degradation in the SII impact observed for high AM values in Fig. 1: both the high magnitude of the SII degradation and its localized effect (by which AM variations mainly affect the visible region of the spectrum), are leading to a significant degradation in the conversion efficiency of MJ solar cells involving a high number of subcells. In this case, the penalty associated with high AM is especially strong due to a) the narrow range of wavelengths converted by each subcell, which may increase the extent to which the spectrum alteration affects the power generated by each individual subcell; and b) the series connection between the subcells, which may give rise to dramatic reduction in the electric power generated, since the current of the whole device is imposed by the lowest current generated by each individual subcell.

### 5.2 *Impact of AOD*

Figure 5 depicts the conversion efficiency of MJ solar cells containing up to 10 subcells as a function of AOD. Single-junction cells show a limited sensitivity to AOD. For a considerable increase of AOD between 0 and 1, the decrease in conversion efficiency is then less than 3% relative to the peak conversion efficiency attained at low AOD. Conversely, MJ solar cells experience a dramatic decrease in their maximum efficiency when exposed to high AOD, in a way similar to that caused by an increasing AM. In particular, for AOD larger than ≈0.6, the efficiency of MJ stacks involving 5 subcells or more appears comparable to, or even lower than, the efficiency of dual or triple junction solar cells.

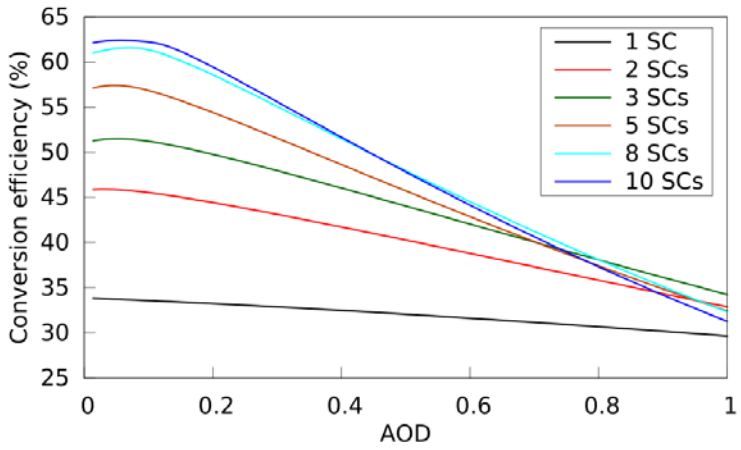


Figure. 5 Conversion efficiency of "AM1.5D-optimized" MJ Solar cells comprising up to 10 subcells (SC) as a function of Aerosol Optical Depth (AOD).

As already mentioned, variations in the Ångström exponent affect SSI only very moderately, resulting in only a minor drop in conversion efficiency of the MJ solar cells investigated in this study (~1% absolute efficiency decrease in the case of a 10-SC MJ solar cells for $\alpha$ varying from 0 to 2.5). Conversely, the pronounced degradation in the SII impact associated with increasing AOD, portrayed in Fig. 2, leads, together with the increased sensitivity of current-constrained MJ solar cells, to a drop in the conversion efficiency with an amplitude that is a function of both the number of subcells involved in the stack and the AOD value.

### 5.3 *Impact of precipitable water*

PW has been shown to affect the power response of a CPV module, but with a weaker intensity than other factors [9]. Figure 6 shows the PW dependence of the conversion efficiency of MJ solar cells containing up to 10 subcells. As with AM and AOD, cell architectures involving a large number of subcells show a stronger dependence to PW than single-junction solar cells. Each cell architecture investigated here, except single cells, shows a decrease in efficiency for large PW values. Cell architectures involving up

to 5 subcells yield a stable conversion efficiency over a broad range of PW values (between 1 and 5 cm). In contrast, MJ cells made of more than 8 subcells are characterized by a significant decrease in efficiency on either side of the optimum PW (≈1.8 cm), which is close to the reference value (1.416 cm).

These trends differ significantly from those observed when varying AM (Fig. 4) or AOD (Fig. 5). The origin of this discrepancy lies in both the limited impact of PW on spectral irradiance and its different wavelength dependence (as already portrayed in Fig. 3)

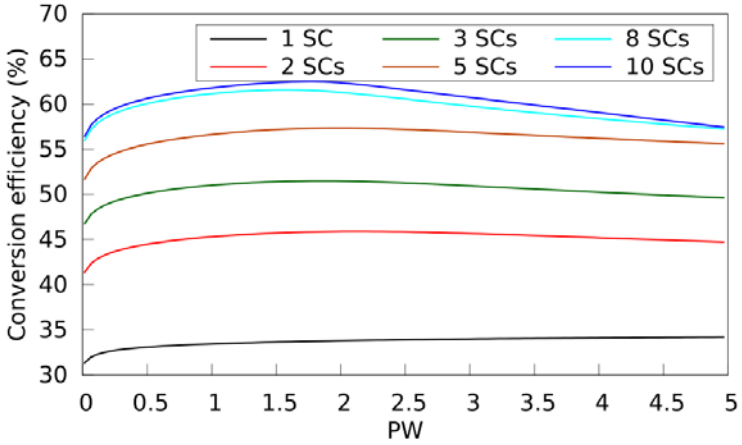


Figure. 6 Conversion efficiency of "AM1.5D-optimized" MJ Solar cells comprising up to 10 subcells (SC) as a function of precipitable water (PW).

From the above results, it can be concluded that the higher the number of subcells in the stack, the narrower the range of spectral characteristics for which the cell performs optimally.

## 6. Spectral simulation

To complement the findings obtained above, more realistic simulations are performed in this section, using long time series of actual measurements of the main atmospheric variables at widely different sites. The direct normal irradiance spectrum is calculated here with the SMARTS radiative model [12], whose main input parameters are the atmospheric variables defined above (AM, AOD, PW, $\alpha_1$ and $\alpha_2$), as well as station pressure, $p$, and ozone amount, $u_o$. The AM values are calculated in SMARTS from the solar zenith angle ($Z$) for the location and time considered.

Simultaneous values of $Z$, AOD, PW, $\alpha$, $p$ and $u_o$ are obtained from the Aerosol Robotic Network (AERONET) database [14]. Its AOD at 500 nm is used here, while its default $\alpha$ value (obtained between 440 and 870 nm) provides both the $\alpha_1$ and $\alpha_2$ values required by SMARTS. This simplification is adopted here because (i) the single-$\alpha$ model is closer to the original Ångström definition; and (ii) experimental errors associated with small-band determinations of the AOD variation are decreased [11].

AERONET's level 2.0 data are used exclusively here to guarantee the highest possible data quality (after cloud screening, calibration and degradation correction). The main filtering criterion (cloud screening) is based on the stability of AOD during 1-minute test periods. It effectively removes nearly all data points that are impacted by the passage of thin or thick sun-obscuring clouds [15].

Because the precise estimation of a solar cell's energy output requires detailed information on the sunlight spectrum throughout at least a whole year, a preliminary examination of the available datasets in some public-domain databases (such as the Baseline Surface Radiation Network (BSRN) [16]) has been made to select only those locations and years with a high density of measured data, including DNI and AERONET's atmospheric retrievals. The latter are performed every ≈15 minutes for AM less than 5. Following the procedure described by Chan et al. [9], measurement gaps longer than 15 minutes are considered to be the signature of extended cloudiness. The corresponding data were thus not taken into account in the simulations.

### 6.1 *Selected locations*

Six different locations were selected according to three criteria: (i) They should be representative of the large range of climatic conditions on the planet; (ii) They should provide high-quality data over an extended period of time (a constraint satisfied by only a small fraction of AERONET sites); and (iii) They should have co-located and simultaneous DNI measurements, in order to validate the simulated spectra.

The selected stations cover a wide range of latitudes (see details in Table 2), extending from Nauru (near the equator) to Palaiseau (near Paris, France). Xianghe (China) is characterized by a high pollution level resulting in systematically large AOD. In contrast, the high elevation of Izaña's mountain site (Tenerife, Spain) is characterized by a generally very low background AOD level, with occasional dust episodes from the Sahara. Nauru and Ilorin are tropical sites with high PW, as opposed to arid sites, such as Sede Boqer, Solar Village, or Izaña. The latter is the driest due to its high elevation. Sede Boqer (Israel) and Solar Village (Saudi Arabia) are characterized by intermediate values of all variables, with however large daily excursions in AOD and $\alpha$ in the wake of regional dust storm activity.

Data breaks due to the lack of AERONET data for AM >5 amount to less than 8% at any site and 4.2% overall, with Izaña (7.72%) and Palaiseau (7.01%) showing the most pronounced amounts of missing data. Table 2 summarizes the geographic coordinates and the elevation of the selected sites, jointly with the year selected for running the simulation (chosen for the best availability of both AERONET data and DNI measurements). Table 2 also includes typical values of the mean daily DNI at each selected location, retrieved from the Solar and Wind Energy Resource Assessment (SWERA) database [17]. According to these values, only 4 of the selected sites are likely to be suitable for CPV operation. In particular, the limited solar resource in Palaiseau and Xianghe would probably avoid considering CPV systems as a realistic option for electricity production.

However, because of the extreme AM (Palaiseau) and AOD (Xianghe) typical of these two cities, including them in this study allows a deeper understanding of how MJ solar cells can accommodate spectral characteristics extending beyond values typically encountered at locations considered as suitable for CPV.

Table 2: Cumulated direct beam irradiances simulated for the selected locations.

| Simulated year | Location | Latitude (°) | Longitude (°) | Elevation (m) | Mean daily DNI (kWh/m²/day) [17] |
|---|---|---|---|---|---|
| 2013 | Izaña | 28.31 | -16.50 | 2373 | 6.5-7.0 |
| 2011 | Nauru | -0.52 | 166.92 | 7 | 6.0–6.5 |
| 2012 | Palaiseau | 48.71 | 2.21 | 156 | 3.0–3.5 |
| 2004 | Sede Boqer | 30.86 | 34.78 | 480 | 6.0–6.5 -> 6.5-7.0 |
| 2001 | Solar Village | 24.91 | 46.40 | 768 | 6.5-7.0 |
| 2009 | Xianghe | 39.75 | 116.96 | 32 | 5.5-6.0 |

Figure 7 illustrates the monthly variation of the most representative atmospheric parameters obtained by AERONET at the selected locations. These graphs conveniently display the amplitude with which each variable varies throughout the simulation year.

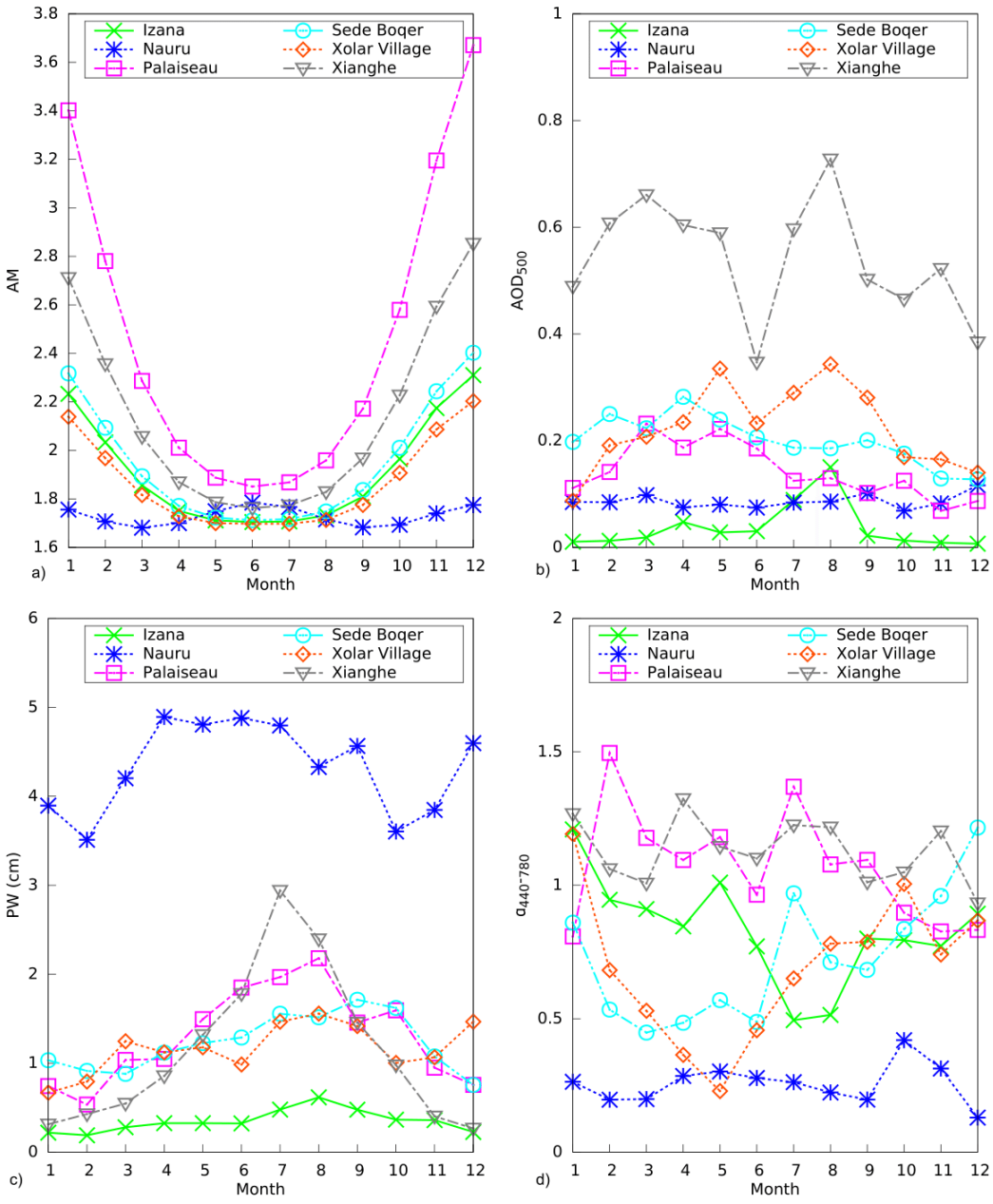


Figure. 7. Monthly-average values of the main atmospheric variables for the simulated sites, obtained from AERONET. In the case of AM, the values are limited to AM < 5, in agreement with AERONET measurements.

The mean-annual observed values of the main atmospheric variables also appear in Table 3, illustrating some noticeable features for each investigated location. For instance, both AM's magnitude and amplitude of its variation over the course of a year are a direct function of latitude, as could be expected (Fig. 7). High monthly and annual AOD values occur at sites that are more or less regularly impacted by pollution, dust or smoke. Such high mean values also indicate an underlying large daily variability [18]. The low mean annual $\alpha$ values reported at Nauru and Solar Village characterize the prevalence of maritime aerosols at the former site, and of a mixture of desert dust at the latter site. Conversely, the large $\alpha$ values observed at Palaiseau and Xianghe are related to the

prevalence of urban pollution there. Finally, the PW annual mean value is clearly related to the specific climate of each site. At the two extremes are Izaña and Nauru. Because PW is a direct function of temperature, it is normally higher in summer than winter, and is always high in the Tropics (Fig. 7).

Table 3: Annual mean values of the main atmospheric variables

| | **Izaña** | **Nauru** | **Palaiseau** | **Sede Boqer** | **Solar Village** | **Xianghe** |
|---|---|---|---|---|---|---|
| **AM** | 1.89 | 1.72 | 2.29 | 1.92 | 1.85 | 2.07 |
| **AOD** | 0.04 | 0.09 | 0.16 | 0.18 | 0.24 | 0.53 |
| **PW (cm)** | 0.37 | 4.17 | 1.44 | 1.34 | 1.18 | 1.01 |
| **α** | 0.80 | 0.26 | 1.15 | 0.86 | 0.64 | 1.12 |

### 6.2 *Direct normal irradiance validation*

The validation of the spectra generated by SMARTS is undertaken by comparing the calculated broadband DNI to reference irradiance measurements obtained from the Baseline Surface Radiation Network (BSRN) [16]. A good agreement is achieved between the simulated and the measured data, as depicted in Figs. 8, 9, and 10, showing the irradiance profiles for three selected locations, namely Sede Boqer (Fig. 8), Solar Village (Fig. 9), and Xianghe (Fig. 10), and two different typical days. It should be stressed that the large drops in the measured data, due to clouds obscuring the sun, are not modeled in the simulations.

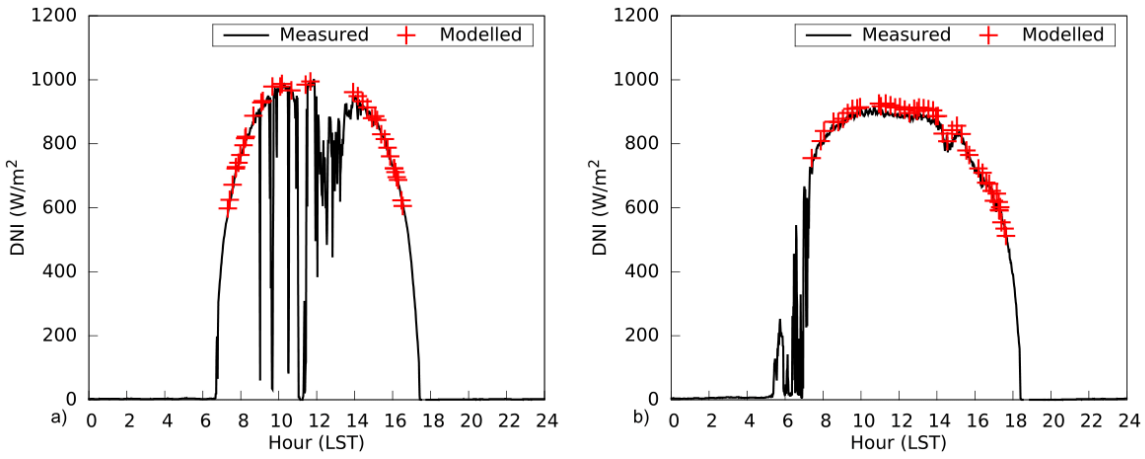


Figure.8. DNI at Sede Boqer on 20 February (left) & 28 July (right), 2004.

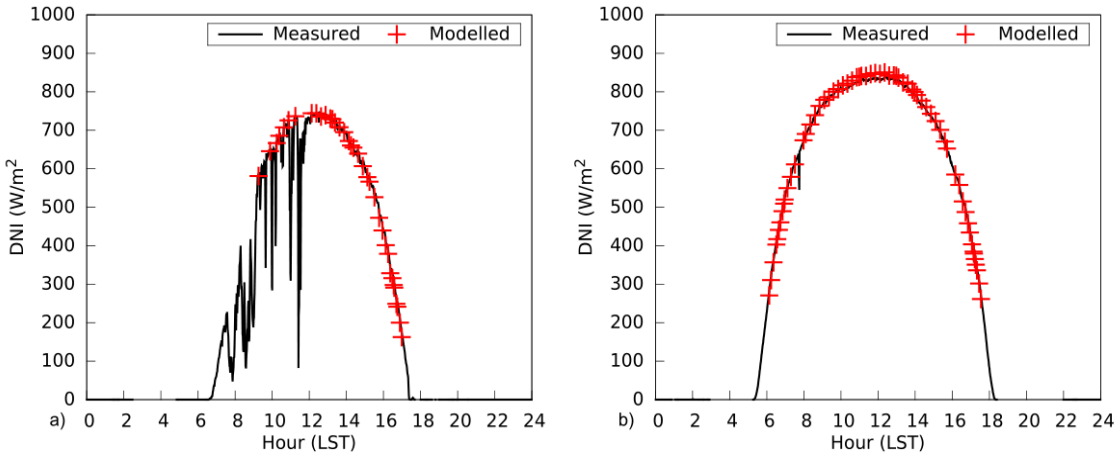


Figure.9. DNI at Solar Village on 15 May (left) and 26 February (right), 2001.

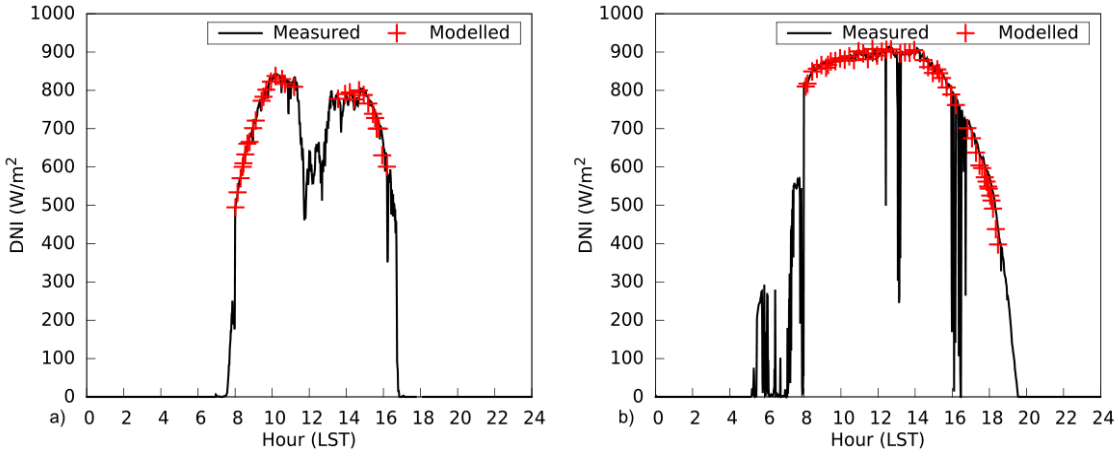


Figure.10. DNI at Xianghe on 10 June (left) and 25 February (right), 2009.

## 7. Results

Figure 11 shows the averaged and expected conversion outputs of a CPV system calculated over a whole year, and for each location considered in this study.

For the sake of clarity, the energy output for each of the architectures studied here is normalized relatively to the energy output of a single-junction solar cell. (As a consequence, the reference value of 1 corresponds to the energy output achievable using CPV systems equipped with single-junction solar cells.) The blue-grey bars depict the mean electricity output achievable with each one of the cell architecture considered, whereas the green bars show the expected energy output, assuming that, when adding an extra junction to the stack, the gain in the energy output follows the efficiency enhancement reported in Table 1.

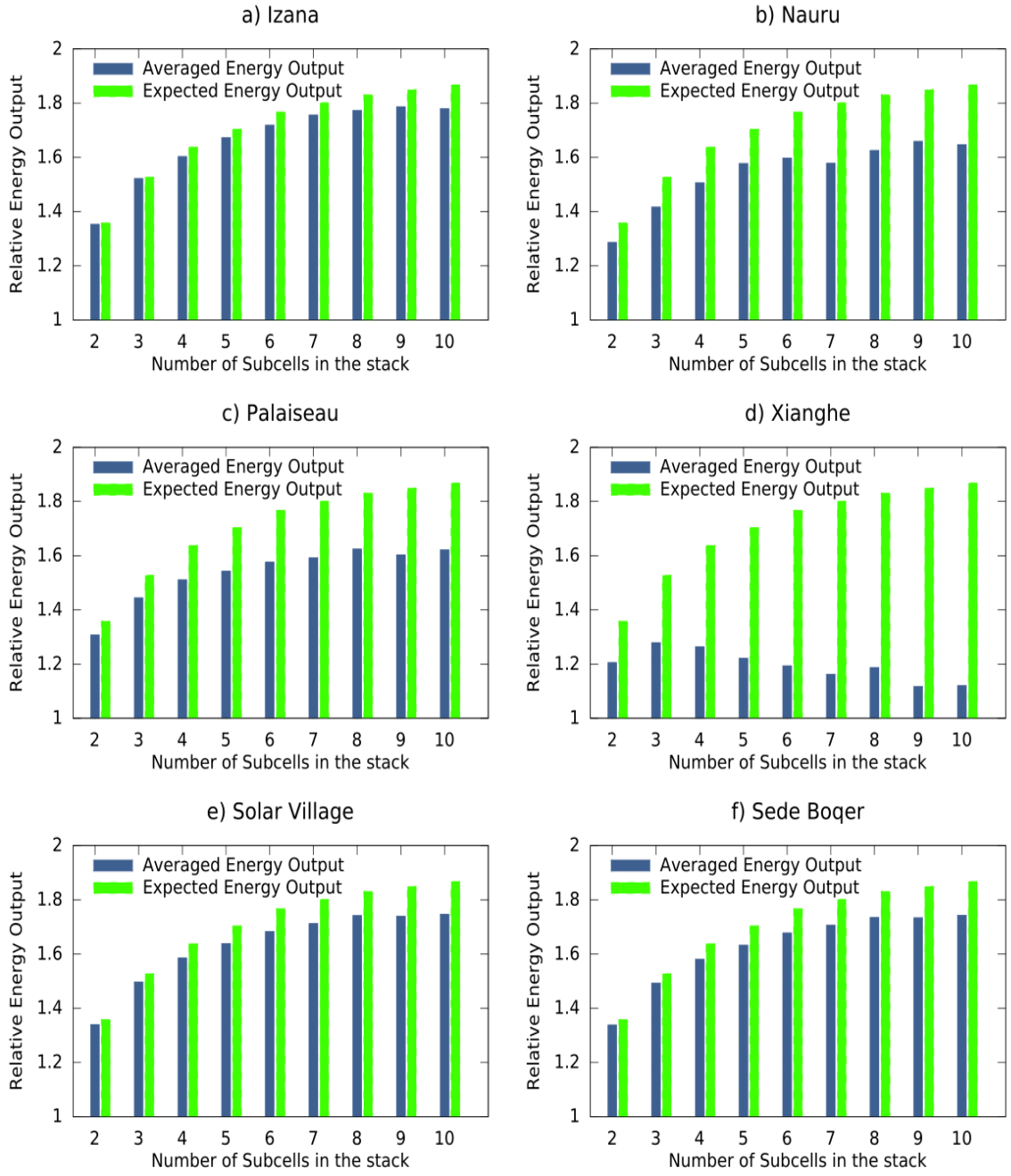


Figure. 11. Averaged energy (blue-grey bars) and expected energy output (green bars) of CPV systems involving MJ solar cells comprising up to 10 subcells, for each location investigated in this study. The energy output is normalized relatively to the annual energy yield of a CPV system based on single-junction solar cells.

As could be expected from the results in Section 5, the variations in CPV module energy output are especially large for modules based on MJ cells involving a high number of subcells. Furthermore, it should be stressed that: a) the difference between the averaged energy output and the expected energy output is always increasing with increasing number of subcells in the stack, for any location; and b) the gain in energy output observed when increasing the number of subcells is strongly dependent on location.

Sites characterized by high daily-mean DNI, such as Izaña, Nauru, Sede Boqer or Solar Village, globally demonstrate the highest benefit in terms of energy yield when the number of subcells increases. Still, despite the favorable solar resource at these four sites, some differences can be observed. In particular, the gain in energy output appears particularly strong at Izaña. It very closely follows the expected energy output for MJ cells made of 2 or 3 subcells, and still represents a significant fraction of the expected energy output for cell architectures involving 4 subcells or more. (Note, however, the very modest energy increases beyond 7 subcells.) These trends are largely attributable to the very low PW and AOD values there, which, together with the moderate mean AM value, explain the significant gain in energy output attainable with MJ cells comprising a high number of subcells.

Solar Village and Sede Boqer are located in similar desert environments and thus show comparable spectral characteristics, i.e., intermediate values of AM, $AOD_{500}$, and PW compared to the other sites. This similitude explains the similar behavior of these two sites with regard to the energy gain resulting from an increased number of subcells. Remarkably, even though the improvement in energy output is significant, the difference between expected and averaged energy output is more pronounced than at Izaña. At the two desert sites, using MJ cells involving more than 7 subcells only brings a small or negligible increase in energy output of the system.

The extent to which PW affects the energy yield over the course of a year is illustrated in Fig. 11b, based on the case of a conceptual system installed in tropical Nauru. Despite its low latitude and low aerosol level, the energy output only shows a modest improvement when subcells are added to the MJ stack. Both Xianghe and Palaiseau are characterized by low mean daily DNI, high AM and moderate PW values. However, Xianghe is characterized by a much higher pollution level and higher AOD compared to Palaiseau. The steeply decreasing energy output for MJ cell architectures involving more than 3 subcells is a result of these adverse conditions at Xianghe. The Xianghe result stress the fundamentally negative impact that high AOD is likely to have on the energy output achievable using advanced MJ cell architectures.

Figure 12 shows the variation in annual energy yield for MJ cell architectures comprising up to 10 subcells, averaged over the 6 selected sites.

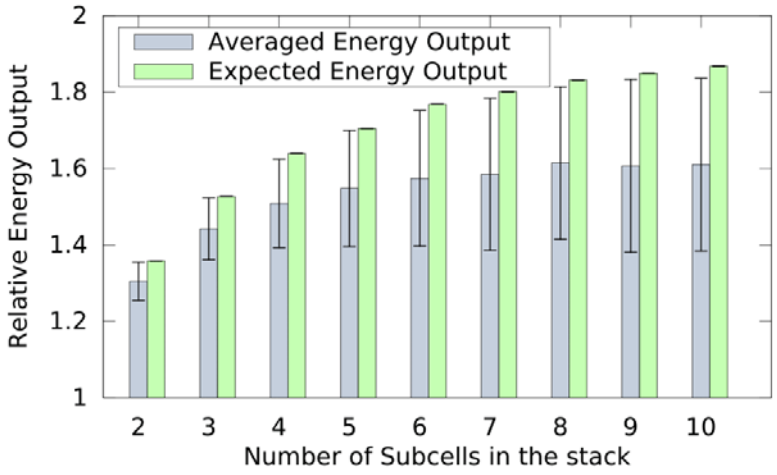


Figure. 12 Averaged energy (blue-grey bars) and expected energy output (green bars) of CPV systems involving MJ solar cells comprising up to 10 subcells. The energy output is normalized relatively to the annual energy yield of a CPV system using single-junction solar cells. The standard deviation showing the variance induced by location-specific effects is also displayed.

Globally, multi-junction solar cells involving between 2 and 6 subcells show a significant increase in the annual energy output relatively to the reference “single-junction” system. Conversely, cell architectures involving more than 6 subcells demonstrate a very modest increase in energy output on average, relative to MJ cells comprising 5 subcells. A slight decrease in energy output can even be observed when the number of subcells exceeds 8. The gap between the average and the expected energy output increases with increasing number of subcells in the stack. The gain in peak efficiency obtained by adding extra subcells does thus not necessarily translate in actual annual yield gains in MJ cells involving 6 subcells or more.

## 8. Statistical distribution of the energy output

At first glance, the performance of a given MJ cell architecture—defined as its ability to maximize energy production over an extended period of time—can be assessed from its capacity to efficiently convert sunlight into electricity, which in turn can be evaluated by the difference between the averaged and the expected energy output shown in Fig. 12. Another important element to consider, however, is the range of spectral conditions that it can accommodate without any significant decrease in energy output. In this sense, the raw energy yield under *standard* conditions does not represent an appropriate quantity to evaluate energy performance, since its value does not account for any variation in energy output from one site to another, which can be substantial. The significant variance in annual system performance induced by location-specific effects is discussed below.

A smooth increase in the mean standard deviation of the energy output can be observed as a function of the number of subcells in the stack (Fig. 12). This behavior is a signature of the increased sensitivity of MJ solar cell architectures involving multiple subcells to

variations in the spectral distribution of sunlight. Even though an increase in the number of subcells in a MJ stack is likely to lead to an increased energy output (as illustrated in Fig. 12), the standard deviation appears to exceed 0.1 for MJ solar cell architecture comprising 4 subcells or more, making the energy output of these systems less predictable, and highly dependent on the geographic location where the system is actually installed.

The main findings of this analysis are summarized in Table 4. In particular, it can be seen that the standard deviation of a 9-cell or 10-cell system is nearly three times larger than that of a "conventional" triple-junction cell, whereas their average annual input is only increased by ~12%.

Table 4: Expected efficiency gain and averaged energy output relative to a single-junction solar cell based CPV module. Both the efficiency and the energy output (averaged over the 6 sites studied) are normalized to the single-junction cell reference value.

| **Number of subcells** | **Expected efficiency gain as compared to single-junction cell** | **Averaged annual energy output as compared to single-junction cell** | **Standard Deviation** |
|---|---|---|---|
| **1** | — | 1 | 0 |
| **2** | +35.9% | +30.5% | 0.05 |
| **3** | +52.7% | +44.2% | 0.08 |
| **4** | +63.9% | +50.8% | 0.12 |
| **5** | +70.5% | +54.8% | 0.15 |
| **6** | +76.8% | +57.4% | 0.18 |
| **7** | +80.1% | +58.5% | 0.20 |
| **8** | +83.1% | +61.4% | 0.20 |
| **9** | +84.9% | +60.7% | 0.23 |
| **10** | +86.7% | +61% | 0.23 |

## 9. Effect of luminescent coupling

Luminescent coupling between the subcells of an MJ stack (i.e., the radiation emitted by a subcell and absorbed by a neighboring junction) is known to mitigate the effects of spectral variation in the incident sunlight [19][20].

Accounting for the luminescent coupling between the subcells of an MJ solar cell can be simply achieved by adding a supplementary term to Eq. 1, with the purpose of evaluating the fraction of light emitted by a subcell and absorbed by the junction underneath [20].

Figure 13 shows the improvement in energy output of a CPV system based on MJ solar cells comprising up to 10 subcells, when taking into account this luminescent coupling between all subcells. The bars show the improvement in efficiency relative to the "reference" case, for which no luminescent coupling is considered. (The calculations are made here assuming a thick-cell scenario, as well as a coupling coefficient of 0.9, corresponding to a strong coupling efficiency between the subcells of the stack.)

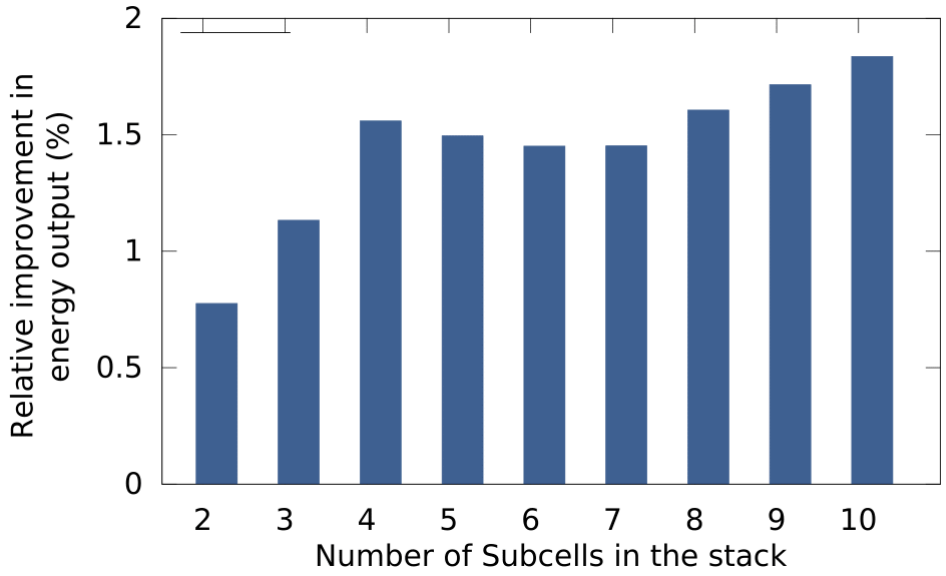


Figure. 13. Relative improvement in the energy output of a CPV system comprising up to 10 subcells, considering a strong luminescent coupling between the subcells of the stack, and assuming an AM1.5D solar spectrum.

Luminescent coupling is shown to result in a slight improvement in the energy output of CPV systems. The gain in energy yield increases for increasing number of junctions in the stack, attaining almost 2% in the case of a 10-junction solar cell. Note the substantial improvement from 2 to 4 junctions, followed by quasi-stagnation beyond 4 subcells: despite the noticeable effect of luminescent coupling, the associated gain in energy output is far from counter-balancing the negative impact of AOD, AM, or PW reported above.

## 10. Discussion and conclusions

Increasing the number of subcells in an MJ stack is known to lead to increased conversion efficiency, because of the better exploitation of the broad range of photonic energy in the solar spectrum. However, the present results suggest that this theory-based statement is not necessarily verified in practice when considering the energy output of a CPV system in operation over a whole year. A noticeable improvement in energy output of a CPV module using tandem or triple-junction solar cells (relative to single-junction solar cells) is expected, but this gain becomes highly location-dependent for CPV modules comprising 4 subcells or more. In particular, the following conclusions are worth to be emphasized:

1) The use of MJ cells involving 4 subcells or more does not guarantee a higher annual energy output. The latter's sensitivity to variations in the spectral distribution of sunlight is shown to be particularly pronounced for cell architectures involving a high number of subcells. As a consequence, the ability of these MJ architectures to accommodate changes in the spectral content is relatively weak, explaining the trends observed and the inability of these cells to achieve the expected energy output over a long period.

2) The gap between the simulated annual energy output and the expected (theoretical) energy output appears to grow steadily when the number of subcells increases in the stack, even at sites with the most favorable solar resource.

The above conclusions raise a critical question about *how* advanced MJ solar cells that include a large number of subcells should be rated or qualified. Is it still relevant to consider the solar-to-electricity conversion efficiency as the sole indicator of the cell's ability to efficiently convert photons into electricity? The present results suggest that the capacity to optimally generate energy throughout an extended period of time, representative of actual operating conditions, should be carefully evaluated. Whereas the efficiency of CPV cells can be rated against a unique set of standard conditions, their actual annual output is a complex function of the number of subcell and of local atmospheric conditions. This type of analysis should be refined with more detailed simulations of the energy output of current or future generations of MJ solar cells involving a high number of subcells.

The present results indicate that an optimal MJ architecture could have between 4 and 7 subcells. Beyond 7 subcells, the slight gains in peak efficiency are likely outweighed by detrimental increases in dependence on local conditions and in annual yield variability: if places suitable for CPV do show a real improvement in terms of energy yield when using MJ cells comprising increasing number of subcells, the benefit for implementing additional subcells becomes much weaker in the case of sites characterized by less favorable solar resources. This last point raises the question of the extent to which a fine-tuning of the cell architecture could lead to improvement in the energy output of CPV systems. Finally, luminescent coupling can mitigate the adverse effects of high air mass, high aerosol optical depth, or variable precipitable water, only to a limited extent.

## Acknowledgements

This work was supported in part by the Program “Investment for the Future” of the National Agency for Research of the French State under award number ANR-10-LABX-22-01-SOLSTICE and by “Ministerio de Economía y Competitividad“ of Spain under grant numbers ENE2013-48325-R and BES-2014-069596. We thank the AERONET staff for establishing and maintaining the AERONET sites investigated in this study. We also thank the Baseline Surface Radiation Network and their staff for providing high quality data. Finally, we also would like to thank Laurent Lestrade and Yann Volut for their technical assistance.

## References

1. Pérez-Higueras P, Fernández EF. High Concentrator Photovoltaics, Springer International Publishing: Cham, 2015; 1-8.
2. Press Release, Fraunhofer Institute for Solar Energy Systems , 1 December 2014 (accessed at https://www.ise.fraunhofer.de/en/press-and-media/press-releases/press-releases-2014/new-world-record-for-solar-cell-efficiency-at-46-percent
3. Chiu PT, Law DC, Woo RL, et al. Direct Semiconductor Bonded 5J Cell for Space and Terrestrial Applications. IEEE Journal of Photovoltaics 2014; **4** (1): 493–497.
4. Vos AD. Detailed balance limit of the efficiency of tandem solar cells. Journal of Physics D: Applied Physics 1980; **13**: 839-846.
5. Martí A, Araújo GL. Limiting efficiencies for photovoltaic energy conversion in multigap systems. Solar Energy Materials and Solar Cells 1996; **43**: 203–222.
6. Vossier A, Al Alam E, Dollet A, Amara M. Assessing the Efficiency of Advanced Multijunction Solar Cells in Real Working Conditions: A Theoretical Analysis. IEEE Journal of Photovoltaics 2015; **5** (6): 1805–1812.
7. Shockley W, Queisser HJ. Detailed balance limit of efficiency of p-n junction solar cells. Journal of Applied Physics 1961; **32**: 510–519.
8. Brown AS, Green MA. Detailed balance limit for the series constrained two terminal tandem solar cell. Physica E: Low-dimensional Systems and Nanostructures 2002; **14**: 96–100.
9. Chan NLA, Brindley HE, Ekins-Daukes NJ. Impact of individual atmospheric parameters on CPV system power, energy yield and cost of energy. Progress in Photovoltaics: Research and Applications 2014; **22**: 1080–1095.
10. Eck TF, Holben BN, Reid JS, Dubovik O, Smirnov A, O’Neill NT, Slutsker I, Kinne S. Wavelength dependence of the optical depth of biomass burning, urban,

and desert dust aerosols. Journal of Geophysical Research: Atmospheres 1999; **104** (D24): 31333–31349

11. Jaus J, Gueymard CA. Generalized spectral performance evaluation of multijunction solar cells using a multicore, parallelized version of SMARTS. AIP Conference Proceedings 2012; **1477**: 122–126.

12. Gueymard CA. Parameterized transmittance model for direct beam and circumsolar spectral irradiance. Solar Energy 2001; **71** (5): 325–346

13. ASTM, 2004. G173-03 Standard tables for reference solar spectral irradiances: direct normal and hemispherical on 37° tilted surface. Book of Standards Volume: 14.04, American Society for Testing and Materials, West Conshohocken, PA

14. Aerosol Robotic Network (AERONET) homepage. http://aeronet.gsfc.nasa.gov

15. Holben BN, Eck TF, Slutsker I, Tanré D, Buis JP, Setzer A, Vermote E, Reagan JA, Kaufman YJ, Nakajima T, Lavenu F, Jankowiak I, Smirnov A. AERONET—A Federated Instrument Network and Data Archive for Aerosol Characterization. Remote Sensing of Environment 1998; **66** (1): 1–16.

16. World Radiation Monitoring Center – Baseline Surface Radiation Network homepage. http://bsrn.awi.de/

17. Solar and Wind Energy Resource Assessment (SWERA) homepage. https://maps.nrel.gov/swera

18. Gueymard CA. Temporal variability in direct and global irradiance at various time scales as affected by aerosols Solar Energy 2012; **86** (12): 3544–3553.

19. Friedman DJ, Geisz JF, Steiner MA. Effect of Luminescent Coupling on the Optimal Design of Multijunction Solar Cells. IEEE Journal of Photovoltaics 2014; **4** (3): 986–990.

20. Chan NLA, Thomas T, Fuhrer M, Ekins-Daukes NJ. Practical Limits of Multijunction Solar Cell Performance Enhancement From Radiative Coupling Considering Realistic Spectral Conditions. IEEE Journal of Photovoltaics 2014; **4** (5): 1306–1313.